Oceanic carbon and water masses during the Mystery Interval: A model-data comparison study

W. N. Huiskamp[1] and K. J. Meissner[1]

Received 27 June 2012; revised 27 September 2012; accepted 2 October 2012; published 14 November 2012.

[1] The 'Mystery Interval' (17.5–14.5 ka BP) is characterized by a large decline in atmospheric $\Delta^{14}C$ synchronous with an increase in atmospheric CO_2. The most widely accepted hypothesis to explain these observed shifts involves the existence of an isolated 'old' ocean carbon reservoir that was subsequently ventilated. Here we use the UVic Earth System Climate Model to locate a potential carbon rich and $\Delta^{14}C$ depleted water mass under 17.5 ka BP boundary conditions. We then investigate two mechanisms for the potential ventilation of such a reservoir, namely the weakening of the North Atlantic Meridional Overturning due to iceberg calving and latitudinal shifts in Southern Hemisphere Westerlies (SHW) due to southern hemispheric warming. We find that simulations derived from an equilibrium state forced with present-day SHW and moderate North Atlantic Deep Water (NADW) formation are in better agreement with atmospheric and ocean $\Delta^{14}C$ reconstructions than simulations derived from an equilibrium state forced with a northward shifted SHW belt resulting in a shut-down of the Atlantic Meridional Overturning and formation of North Pacific Deep Water. For simulations with present-day SHW, the oldest water masses are found in the North Pacific, although the Southern Ocean cannot be ruled out as a potential 'Mystery Reservoir'. According to our simulations, the strength of Atlantic overturning is the dominant mechanism in increasing the ocean-atmosphere carbon flux, while shifting SHW results in a rearrangement of deep ocean carbon largely between the Atlantic and Pacific basins. In our 'best case' scenario, the model can account for 58% of the atmospheric CO_2 increase and 48% of the atmospheric $\Delta^{14}C$ decline. While the rate of ventilation and the age of ventilated water masses are comparable with observations, the ventilation in the model could not be sustained long enough to account for the full excursion seen in paleodata.

Citation: Huiskamp, W. N., and K. J. Meissner (2012), Oceanic carbon and water masses during the Mystery Interval: A model-data comparison study, *Paleoceanography*, *27*, PA4206, doi:10.1029/2012PA002368.

1. Introduction

[2] Paleoclimate-proxy data from the last ~25 kyr BP suggests significant climate change occurring during the transition from the Last Glacial Maximum spanning 26.5–19 ka BP (LGM) [*Clark et al.*, 2009] to present-day conditions [*Clark et al.*, 2012]. Major events include the Heinrich 1 (H1) event at 16.8 ka BP [*Hemming*, 2004], the Bølling-Allerød (B-A) event at 14.6–12.8 ka BP and the Younger Dryas (YD) at 12.9–11.5 ka BP. Of particular interest is the 'Mystery Interval', a period of time spanning 17.5–14.5 ka BP, which saw cooling of the Northern Hemisphere (NH) [*Bard et al.*, 2000; *Grootes et al.*, 1993], a significant weakening of the North Atlantic Meridional Overturning Circulation (AMOC) [*McManus et al.*, 2004], Southern Hemisphere warming [*Morgan et al.*, 2002], changes in atmospheric circulation [*Toggweiler et al.*, 2006, and references therein], a rise in atmospheric CO_2 by ~40 ppm [*Monnin et al.*, 2001] and a significant reduction of ~190‰ in the atmospheric $\Delta^{14}C$ record [*Broecker and Barker*, 2007; *Reimer et al.*, 2009]. Potential changes in ^{14}C production rates based on paleomagnetic and sedimentary ^{10}Be reconstructions can only account for approximately of 37‰ of the observed ^{14}C reduction, whereas ice core ^{10}Be reconstruction cannot account for any of the $\Delta^{14}C$ excursion [*Broecker and Barker*, 2007]. Conversely, a modeling study by *Köhler et al.* [2006] suggests changes in production rate to play a significant role during the interval, allowing for a maximum carbon cycle contribution of roughly 100‰. *Köhler et al.* [2006] show there is indeed a high level of uncertainty in production estimates, this is supported by *Skinner et al.* [2010], however they suggest that changes in the carbon cycle should account for a minimum of 150‰.

[3] The prevailing theory that seeks to explain this large decrease in $\Delta^{14}C$ is discussed, amongst others, by *Broecker and Barker* [2007] and *Broecker* [2009] and involves the

[1]Climate Change Research Centre, University of New South Wales, Sydney, New South Wales, Australia.

Corresponding author: W. N. Huiskamp, Climate Change Research Centre, University of New South Wales, Sydney, NSW 2052, Australia. (w.huiskamp@unsw.edu.au)

0883-8305/12/2012PA002368

existence of an isolated abyssal carbon rich and ^{14}C deficient ocean reservoir, or 'Mystery Reservoir' (MR), which could potentially account for the observed changes in atmospheric ^{14}C, ^{13}C and CO_2 [*Schmitt et al.*, 2012; *Brook*, 2012]. The proposed MR of *Broecker and Barker* [2007] is stabilized and allowed to remain isolated from the atmosphere for much of the LGM. The theory involves events during the deglaciation prompting the ventilation of this reservoir, increasing atmospheric CO_2 and decreasing $\Delta^{14}C$ synchronously. Some sediment cores and deep-sea corals corroborate this theory and show evidence of very old water masses, namely in the Arabian Sea [*Bryan et al.*, 2010], off Baja California [*Marchitto et al.*, 2007], in the Eastern Equatorial Pacific [*Stott et al.*, 2009], and in the Drake Passage [*Burke and Robinson*, 2012].

[4] Original estimates made by *Broecker and Barker* [2007] limit the reservoir to filling no more than 50% of the ocean, which was then further reduced to 30% by *Broecker et al.* [2008]. The lower limit of this reservoir would be of the order of 15% of the worlds oceans, an unlikely scenario as it involves all the radiocarbon having been decayed [*Broecker et al.*, 2008]. *Broecker and Clark* [2010] note that the reservoir would have to occupy the entire ocean below 3.2 km if it was isolated for a ^{14}C half-life. A reservoir of such immense size would almost certainly be mixed with surrounding water masses due to geothermal heating from below and eddy mixing from above [*Broecker and Clark*, 2010]. *Hain et al.* [2011] use a box model to test this hypothesis and find that no such MR could have existed due to (i) the dissipation of these potential ^{14}C depleted water masses to the rest of the ocean and atmosphere over time and (ii) anoxia within these potential water masses and simultaneous trapping of alkalinity from $CaCO_3$ dissolution. However these mechanisms would lead to an increase in atmospheric CO_2, which is in conflict with observations [*Monnin et al.*, 2001].

[5] Antarctic Bottom Water (AABW) was the densest and saltiest water mass during the LGM [*Zahn and Mix*, 1991; *Adkins et al.*, 2002] and in combination with extensive sea ice cover inhibiting air-sea CO_2 exchange [*Gersonde et al.*, 2003; *Stephens and Keeling*, 2000] would have allowed Southern Ocean waters to potentially become the MR we seek [*Bryan et al.*, 2010; *Skinner et al.*, 2010]. *Marchitto et al.* [2007] report ^{14}C values of intermediate water in the eastern North Pacific dropping by 300‰ during the last deglaciation and hypothesize the Southern Ocean as the source region for these old water masses. *Basak et al.* [2010] measure the neodymium isotopes of fossil fish teeth and debris taken from *Marchitto et al.*'s [2007] core and find that the isotopic signature of the same water mass shows a clear shift toward Southern Ocean values at approximately 18 ka BP, coincident with the decrease in $\Delta^{14}C$. *Mangini et al.* [2010] analyze deep sea corals in the South Atlantic and provide evidence of a weakening or shut down of Antarctic Intermediate Water (AAIW) approximately 2 kyr prior to the H1 event. The timing and magnitude of the $\Delta^{14}C$ decrease in these corals match values found by *Marchitto et al.* [2007] in the North Pacific and by *Stott et al.* [2009] in the eastern Pacific. Finally, *Skinner et al.* [2010] find evidence of an old water mass pre-dating H1 in the Southern Ocean. They conclude that the critical factors involved in the sequestration and ventilation of this water mass are potentially changing Antarctic sea ice extent, as well as changing wind stress of westerlies and their effect on the Antarctic Circumpolar Current and Circumpolar Deep Water stratification.

[6] *Bryan et al.* [2010] argue that the ^{14}C-depleted waters found at intermediate depth in the Arabian Sea cannot have aged 'in situ' due to isopycnal mixing and hypothesize that these water masses must have been formed either in the Southern Ocean or in the North Pacific. The existence of a northern Pacific reservoir is also mentioned as a possibility by *Rose et al.* [2010]. Sediment cores from the southwest Pacific show a 170‰ decrease in intermediate water $\Delta^{14}C$ prior to the atmospheric decrease [*Rose et al.*, 2010] suggesting that carbon ventilated from the abyssal Southern Ocean lost most of its original depleted ^{14}C as a result of exchange and isotopic equilibration with the atmosphere. *Rose et al.* [2010] conclude that the low ^{14}C values recorded by *Marchitto et al.* [2007] may imply the North Pacific basin as a likely source of old carbon. It is also noteworthy that ^{14}C-depleted waters are not observed along the Chile margin [*De Pol-Holz et al.*, 2010], which therefore would make a North Pacific source for *Marchitto et al.*'s [2007] water mass a likely candidate. However, *Lund et al.* [2011] have recently challenged the theory of a deep northeast Pacific reservoir; as data retrieved from their core W8709A-13PC shows higher $^{14}C/C$ ratios than values recorded in *Marchitto et al.*'s [2007] water mass.

[7] The latitudinal location of the Southern Hemisphere Westerlies (SHW) during the LGM is an area of intense debate within the paleo community. Several studies using regional data reconstructions provide evidence suggesting that the SHW were anywhere between 3 degrees [*Hesse*, 1994], 5 degrees [*McGlone et al.*, 2010] or up to 9–10 degrees north of their present-day location [*Moreno et al.*, 1999; *Lamy et al.*, 1999; *Stuut and Lamy*, 2004; *Toggweiler et al.*, 2006]. Conversely, modeling studies suggest either no significant shifts [*Rojas et al.*, 2009] or a southward shift [*Wyrwoll et al.*, 2000]. With the onset of H1 there is evidence of a southward shift of the Inter-Tropical Convergence Zone (ITCZ) [*Peterson et al.*, 2000; *Cheng et al.*, 2009; *Chiang*, 2009; *Anderson and Carr*, 2010] and with it a southward movement of the SHW [*Barker et al.*, 2009]. This would result in enhanced Ekman upwelling, an increased ventilation of Southern Ocean deep waters and an increase in AAIW formation as well as ocean productivity, which is observed in proxy records as an increase in opal flux near Antarctica [*Basak et al.*, 2010; *Rose et al.*, 2010; *Anderson et al.*, 2009].

[8] At the same time, H1 caused an influx of cold, fresh water into the North Atlantic, reducing North Atlantic Deep Water (NADW) formation rates and associated oceanic heat transport to higher latitudes [*Anderson and Carr*, 2010; *McManus et al.*, 2004; *Bard et al.*, 2000]. Many studies call on a bi-polar inter-hemispheric ocean see-saw to link the cooling and slowing of overturning in the North Atlantic associated with the H1 event to warming and changes in ocean circulation in the Southern Hemisphere [*Anderson and Carr*, 2010; *Bryan et al.*, 2010; *Barker et al.*, 2009; *Cheng et al.*, 2009; *Liu et al.*, 2009; *Robinson et al.*, 2005; *Schmittner et al.*, 2003; *Saenko et al.*, 2003; *Broecker*, 1998]. $^{231}Pa/^{230}Th$ ratios [*Mangini et al.*, 2010] along with εNd records from ocean sediments [*Pahnke et al.*, 2008]

corroborate this theory by implying a larger influence of Southern Sourced Water (SSW) during the H1 event. These changes in the location and intensity of ventilation might have an important impact on global atmosphere-ocean carbon fluxes [e.g., *Skinner et al.*, 2010].For example, today NADW draws down ^{14}C from the atmosphere more efficiently than ^{14}C deficient AABW so the observed changes in SSW/Northern Sourced Water (NSW) domination of the glacial-interglacial deep ocean would have an effect on atmospheric ^{14}C [*Robinson et al.*, 2005].

[9] The B-A event marked a resumption of the AMOC and is also the end of the Mystery Interval [*McManus et al.*, 2004]. With this we see an abrupt warming in the North Atlantic in terms of both atmospheric temperatures and SST [*Liu et al.*, 2009] as well as significant SST increases in Pacific marginal seas [*Kiefer and Kienast*, 2005]. Paleodata of increasingly negative carbon isotope ratios and very low Mg/Ca and Ba/Ca ratios from the northern Iberian peninsula between 15.4 and 13.4 ka BP show large increases in temperature and humidity [*Moreno et al.*, 2010]. The B-A occurred synchronously with the Antarctic Cold Reversal (ACR) in the Southern Hemisphere during which time warming in the Southern Ocean paused as did the increase in atmospheric CO_2 [*Monnin et al.*, 2001]. At the same time, evidence is seen off the coast of Baja California of a proportional increase in North Pacific Intermediate Water (NPIW) to AAIW in neodymium isotopic ratio data [*Basak et al.*, 2010].

[10] This study aims to analyze climate simulations of the Mystery Interval in order to identify the location of the oldest simulated water masses. It then tests two potential mechanisms that have been put forward in the literature to account for the ventilation of these water masses causing the observed increase in atmospheric CO_2 and synchronous decrease in atmospheric $\Delta^{14}C$: a southward shift of the SHW and changes in the strength of the Atlantic Meridional Overturning Circulation (AMOC).

2. Methods

[11] This study utilizes the UVic Earth System Climate Model (ESCM) which consists of a series of sub-models coupled together for relevant feedbacks between them. The ocean is represented by the Modular Ocean Model, Version 2 [*Pacanowski*, 1995], an ocean general circulation model. It is coupled to a vertically integrated, two dimensional energy-moisture balance model of the atmosphere. In addition to these, the UVic ESCM includes a dynamic-thermodynamic sea ice model derived from *Semtner* [1976], *Hibler* [1979] and *Hunke and Dukowicz* [1997], a sediment model [*Archer*, 1996] and a dynamic global vegetation model [*Meissner et al.*, 2003a]. The UVic ESCM also includes an improved NPZD (nutrient, phytoplankton, zooplankton and detritus) model with a parameterization of rapid nutrient recycling due to microbial activity [*Schartau and Oschlies*, 2003]. The NPZD model contains two classes of phytoplankton, nutrients (nitrate and phosphate) and the prognostic tracers of oxygen, dissolved inorganic carbon and alkalinity [*Schmittner et al.*, 2008]. A more thorough description of the UVic ESCM can be found in *Weaver et al.* [2001].

[12] The model is driven by insolation at the top of the atmosphere in addition to wind stress and wind fields [*Kalnay et al.*, 1996] both of which vary seasonally. All model components have a resolution of 3.6° in longitude and 1.8° in latitude. During simulations, the model conserves water, energy and carbon to machine precision. Comparisons of the model's results with observations and proxy data show good agreement, good examples are *Weaver et al.* [2001] and *Meissner et al.* [2003a, 2003b].

[13] Two equilibrium simulations are integrated for 12,000 years under boundary conditions corresponding to paleo-year 17.5 ka BP and hereafter referred to as H1 boundary conditions. This includes an atmospheric CO_2 value of 205 ppm [*Smith et al.*, 1999], land ice extent and thickness from a reconstruction by *Peltier* [2002] and orbital parameters corresponding to paleo-year 17.5 ka BP [*Berger*, 1978]. Atmospheric $\Delta^{14}C$ is set to 393‰ [*Reimer et al.*, 2009]. The two simulations differ in their position of SHW: while simulation A-eq is forced with present-day winds, SHW are shifted 9° of latitude north for simulation B-eq. At the end of the equilibrium simulations, trends in deep ocean temperature and dissolved inorganic carbon (DIC) were analyzed to ensure the simulations had reached equilibrium. It was then possible to diagnose the global mean ^{14}C flux into the ocean for the given boundary conditions, this flux was set equal to the ^{14}C production rate at the top of the atmosphere during the sensitivity simulations [*Meissner et al.*, 2003b; *Meissner*, 2007], so that atmospheric $\Delta^{14}C$ could be calculated prognostically. The production rate of ^{14}C for subsequent sensitivity simulations equals 1.74 atoms cm^{-2} s^{-1} for all simulations derived from A-eq and 1.77 atoms cm^{-2} s^{-1} for all simulations derived from B-eq. This is comparable to an estimated modern day global average ^{14}C production rate of 1.64 atoms cm^{-2} s^{-1} [*Kovaltsov et al.*, 2012].

[14] The sensitivity simulations are generated by changing the latitudinal position of the SHW and/or changing NADW formation via the influx of fresh or saline water into the North Atlantic. Please refer to Table 1 for a list of all sensitivity simulations. All 'f' simulations are forced with a fresh water flux into the North Atlantic of 0.12 Sv for a period of 500 years. This time frame was chosen based on *Hemming* [2004] who uses combined ice rafted detritus records to find an average length of 495 ± 255 years for the H1 ice rafting event. After the freshwater 'hosing' the AMOC in the model remains in its inactive state. As there is paleodata evidence that the AMOC must have turned on again at some point after H1, half the freshwater hosing simulations ('f' simulations) are subsequently forced with an unphysical 'salt flux' of -0.12 Sv (or 4.17×10^6 kg s^{-1}) in the same region the fresh water hosing occurred ('fs' simulations). Simulations including the suffix 'ws' in their name are forced with SHW wind stress fields shifted 9° south, 'wn' are forced with SHW shifted 9° north and 'wpd' simulations are forced with present-day wind stress. All sensitivity simulations have then been integrated for an additional 5000 years under fixed boundary conditions.

3. Results

3.1. Equilibrium Simulations

[15] Our two equilibrium simulations differ in their forcing only in the position of the SHW. This difference in dynamical forcing results in two very different states of the

Table 1. List of Simulations[a]

Name	SHW 9° North	SHW PD	SHW 9° South	Fresh Water	Salt After 500 Years
A-eq		X			
B-eq	X				
A-ws			X		
B-ws			X		
B-wpd		X			
A-wpd-fs		X		X	X
B-wn-fs	X			X	X
A-ws-fs			X	X	X
B-ws-fs			X	X	X
B-wpd-fs		X		X	X
A-wpd-f		X		X	
B-wn-f	X			X	
A-ws-f			X	X	
B-ws-f			X	X	
B-wpd-f		X		X	

[a]The label for each simulation includes a maximum of three parts; the simulation it is derived from (A-eq or B-eq), the location of the SHW ('wn' = 9° north of present-day location, 'wpd' = present-day location and 'ws' = 9° south of present-day location), and freshwater forcing in the North Atlantic ('f' for a fresh water flux in the North Atlantic or 'fs' for a fresh and subsequent saline flux). X denotes "yes."

global circulation: while simulation A-eq (with present-day SHW) forms deep water in the North Atlantic, simulation B-eq (with SHW shifted 9° north) forms deepwater in the North Pacific similar to *Saenko et al.* [2004].

[16] The maximum overturning strength in the North Atlantic exceeds 12 Sv in simulation A-eq and Antarctic Bottom Water (AABW) formation is active with a minimum zonally integrated meridional transport of −9 Sv (Figures 1a and 1b). The oldest water in simulation A-eq is found in the Pacific basin with a Δ^{14}C zonal mean value of −46.6‰; it is situated at 2000–4000 m depth, between 0° and 60°N (Figure 2c). The oldest water in the Atlantic Ocean has a Δ^{14}C zonal mean value of 77.31‰ (Figure 2a) and exists between 4000 m and the bottom, between 60°S and 0°.

[17] When compared to simulation A-eq, simulation B-eq displays stronger AABW formation with a minimum zonally integrated meridional transport exceeding −13 Sv. North Pacific Deep Water (NPDW) formation is also quite strong with a maximum overturning strength of 20 Sv (Figure 1c) while there is an absence of NADW formation (Figure 1d). The oldest water in the Atlantic Ocean is located between 40°N and 60°N (Figure 2b) with a minimum zonal mean Δ^{14}C value of −12.64‰, at a depth of 2000–4000 m. Pacific Ocean water masses are younger, with a minimum zonal mean Δ^{14}C value of 50.11‰, located between 30°–60°N at a depth below 3500 m (Figure 2d).

[18] Figure 3 shows the minimum Δ^{14}C value in the water column for both equilibrium simulations. Neither of the simulations depict the Southern Ocean as a likely location for the Mystery Reservoir (MR). AABW formation and AAIW formation are too active in both simulations to allow accumulation of old carbon in the Southern Ocean. Top-to bottom age differences for both simulations are shown in Figure 4.

3.2. Oceanic Carbon Budgets

[19] Table 2 lists the carbon anomalies for each reservoir at the end of our 13 sensitivity simulations when compared to their parent equilibrium simulation. Three major basins were considered; the Atlantic, Pacific and Indian Oceans. In addition, we analyze changes in the carbon content of the shallow and deep ocean, the shallow box spanning from the surface to 980 m in depth while the deep ocean box spans from 980 m to the bottom. Changes in sediment carbon are at least two orders of magnitudes smaller and have therefore not been included in Table 2. The main results of Table 2 are visualised in Figure 5. There are several conclusions that can be drawn from Table 2 and Figure 5:

[20] 1. All simulations derived from equilibrium simulation B-eq gain carbon in the Pacific Ocean due to an increase in NADW formation and decrease in NPDW formation. This carbon originates predominately in the Atlantic Ocean and, to a lesser extent, the Indian Ocean. Only two simulations (B-wpd and B-wpd-f) are characterized by a larger loss of carbon in the Indian ocean when compared to the Atlantic Ocean. In all cases the carbon fluxes between ocean basins are an order of magnitude larger than changes in atmospheric carbon, implying that most of this carbon is exchanged in the intermediate and deep ocean.

[21] 2. There are six simulations showing a significant increase in atmospheric CO_2. Only four out of these six simulate a net transfer of carbon from the ocean to the atmosphere (B-wn-fs, A-wpd-fs, A-ws-fs, A-wpd-f). The three A simulations (A-wpd-fs, A-ws-fs and A-wpd-f) also show a significant increase in terrestrial carbon, while the terrestrial carbon budget of B-wn-fs remains unchanged (−0.4 Pg C). In addition to these four simulations, which are also the only ones showing a significant increase in atmospheric CO_2 (>10 ppm), there are two simulations characterized by a smaller net increase in atmospheric CO_2 (<10 ppm; B-wpd-fs and B-ws-fs). During these simulations ocean carbon increases while terrestrial carbon decreases.

[22] 3. When SHW shift southward and the AMOC is unchanged or weakened, there is a net transfer of carbon from the atmosphere into the ocean with a synchronous carbon loss from land.

[23] 4. The simulations with the largest decrease in atmospheric Δ^{14}C and largest increases in atmospheric CO_2, A-wpd-fs and A-ws-fs, experience the least inter-basin carbon exchange of all 'fs' simulations. Rather than rearranging deep ocean carbon, the old carbon enters the shallow ocean and ventilates.

3.3. Atmospheric CO_2 and Δ^{14}C Records

[24] Three of our sensitivity simulations (A-wpd-fs, A-ws-fs and B-wn-fs) show a large increase in atmospheric CO_2 (>20 Gt C) with the two A simulations exceeding 30 Gt C. A-ws-fs is closest to replicating the magnitude and rate of change of atmospheric Δ^{14}C [*Reimer et al.*, 2009] and CO_2 [*Monnin et al.*, 2004] (see Figure 6); the simulation shows an atmospheric CO_2 increase of 21 ppm over the course of 3000 years, with 20 ppm of that increase occurring over the first 2000 years. This is in contrast to reconstructed atmospheric CO_2 concentrations [*Monnin et al.*, 2004], which show a consistent increase throughout the interval of roughly 36 ppm. The model accounts therefore for 58% of the reconstructed atmospheric CO_2 increase; and the rate of increase during the first 1500 years of integration is

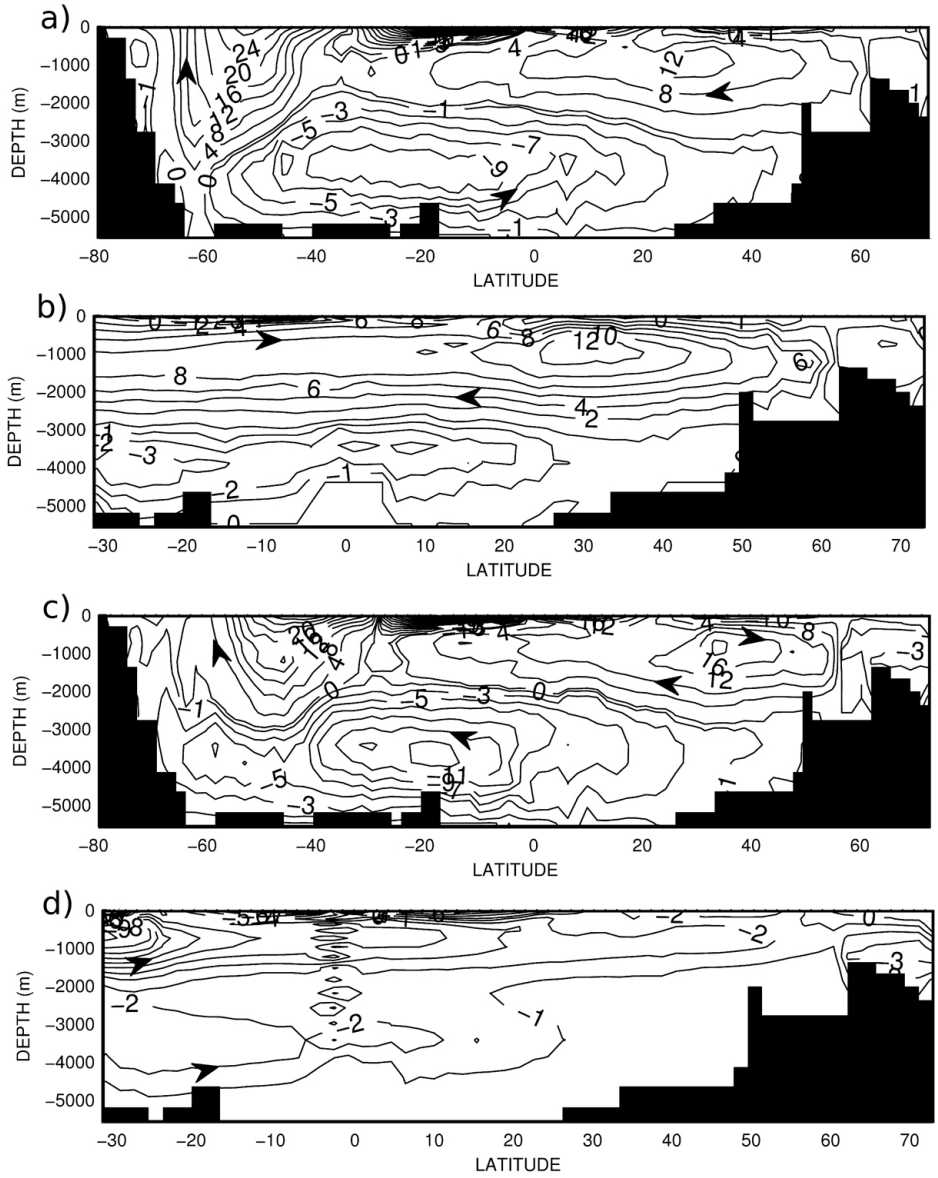

Figure 1. Stream function of the zonally integrated meridional transport for (a) Simulation A-eq - global ocean, (b) Simulation A-eq - Atlantic basin, (c) Simulation B-eq - global ocean and (d) Simulation B-eq - Atlantic basin. Units in Sverdrups.

comparable to the paleo record. Similarly, the simulated atmospheric $\Delta^{14}C$ accounts for 86‰ of the roughly 190‰ decline seen in reconstructed $\Delta^{14}C$ records [*Reimer et al.*, 2009] (Figure 6b). The ventilated carbon may therefore have been slightly 'younger' than expected, as the model accounts for only 45% of the atmospheric $\Delta^{14}C$ decline compared to 58% atmospheric CO_2 increase. Additional data from *Southon et al.*'s [2012] speleothem record (Figure 6b, orange dots) shows a smaller change in $\Delta^{14}C$ during the Mystery Interval when compared to INTCAL09, although this could be due to their record starting its decline 1000 years earlier than INTCAL09, while the total change in the two records is comparable [*Southon et al.*, 2012]. Figure 6 also shows time series derived from simulation A-wpd-fs for comparison (green lines).

3.4. $\Delta^{14}C$ Records in the Ocean

[25] Figure 7 shows time series of ocean $\Delta^{14}C$ for simulations A-wpd-f, A-ws-fs, B-wn-f and B-ws-fs compared to paleo proxy data at five locations in the western Pacific (Figures 7a, 7d, 7g, 7j and 7m) and eight locations in the Eastern Pacific (Figures 7b, 7c, 7e, 7f, 7h, 7i, 7k and 7l). Only four cores have a published record dating just prior to the start of the Mystery Interval (MD01-2416, Figure 7a [*Sarnthein et al.*, 2006]; MD01-2386, Figure 7m [*Broecker et al.*, 2008]; VM21-30, Figure 7k [*Stott et al.*, 2009] and PC08, Figure 7h [*Marchitto et al.*, 2007]). $\Delta^{14}C$ values simulated by equilibrium simulation A-eq are in agreement with reconstructions from cores MD01-2416 [*Sarnthein et al.*, 2006] and PC08 [*Marchitto et al.*, 2007], whereas none of our two equilibrium simulations is in agreement

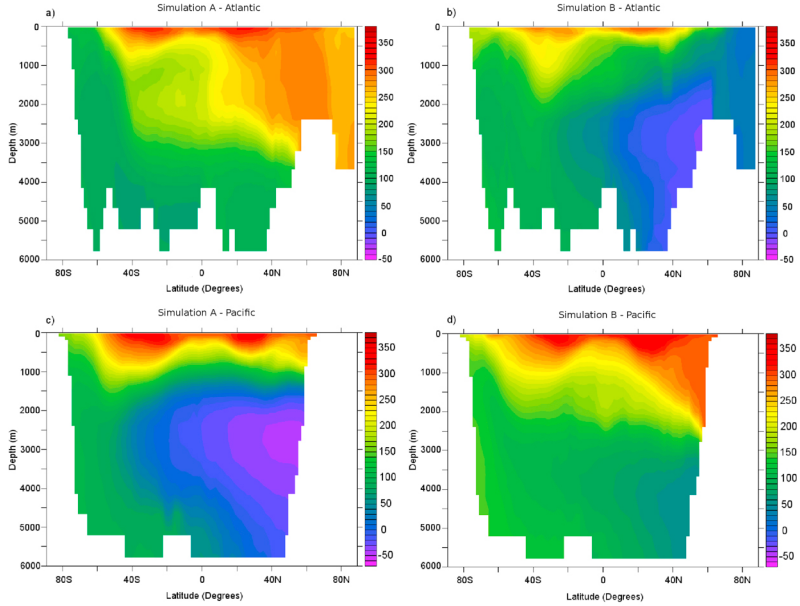

Figure 2. Zonal mean $\Delta^{14}C$ (permil) for equilibrium simulation (a and c) A-eq and (b and d) B-eq. Shown is the Atlantic Ocean (Figures 2a and 2b) and Pacific Ocean (Figures 2c and 2d).

with core MD01-2386 [*Broecker et al.*, 2008] or VM21-30 [*Stott et al.*, 2009]. During the Mystery Interval, no clear conclusions can be drawn as to which sensitivity study is in best agreement with available data. It is noteworthy that none of our simulations are able to replicate the extremely low $\Delta^{14}C$ values recorded in core PC08 [*Marchitto et al.*, 2007] off Baja California (Figure 7h) or in core VM21-30 [*Stott et al.*, 2009] in the equatorial Eastern Pacific (Figure 7k). Similarly, core MD01-2416 [*Sarnthein et al.*, 2006] in the northwest Pacific has three $\Delta^{14}C$ values that are all lower than any of our simulated values at this location (Figure 7a). Cores ODP-887 (Figure 7b [*Galbraith et al.*, 2007]), as well as 1019A01H4 (Figure 7c [*Mix et al.*, 1999]) and W8709-A-13PC (Figure 7e [*Mix et al.*, 1999]), all three located in the northern East Pacific, show one low $\Delta^{14}C$ each that none of our simulations match. On the other hand, the only record in core TR163-31 [*Shackleton et al.*, 1988] in the tropical East Pacific is higher than any of our simulations (Figure 7l). Our sensitivity simulations are simulating $\Delta^{14}C$ values within the error bars for all other cores.

[26] Paleo proxy data from the Atlantic Ocean is compared to four of our simulations in Figure 8. It should be noted that two of the RAPiD cores (Figures 8a and 8b [*Thornalley et al.*, 2011]) have been taken just south of the Greenland-Iceland-Scotland sill, and are compared to model data at depths of 1800 m (Figure 8a) and 1200 m (Figure 8b) due to the coarse resolution of our ocean model. The three RAPiD records show evidence of two distinct water masses; only the younger, better ventilated water mass has values close to the ones replicated in our simulations whereas our model does not capture the very depleted water mass. Similarly, the two coral records at intermediate depth in the southern West Atlantic (C2 and C1, Figures 8i and 8j [*Mangini et al.*, 2010]) each show one record for which $\Delta^{14}C$ is lower than our simulated water masses at that location. Our sensitivity simulations are simulating $\Delta^{14}C$ values within or very close to the error bars for all other cores.

[27] Simulated time series of $\Delta^{14}C$ are also compared to proxy data in the Drake Passage (Figures 9c, 9e, 9f and 9g) and in the southern Atlantic Ocean (Figures 9d and 9h). The A-ws-fs and B-ws-fs simulations both achieve $\Delta^{14}C$ values similar to those recorded in the deep-sea coral [*Goldstein et al.*, 2001] (corresponding to a situation with vigorous overturning circulation in the Atlantic, Figure 9e), although they achieve these values roughly 1000 years late. The A-ws-fs and B-ws-fs simulations are also compatible with one of the dredged deep-sea corals in the Drake Passage (Figure 9c [*Burke and Robinson*, 2012]). However, two dredged corals from a close-by location record much lower $\Delta^{14}C$ values than any of our simulations predict (Figures 9f and 9g [*Burke and Robinson*, 2012]). MD07-3076 (Figure 9h [*Skinner et al.*, 2010]) provides us with a series of records in the South Atlantic throughout the Mystery Interval that are, save for the last one, all well below any of the simulated values; and TN057-21 (Figure 9d [*Barker et al.*, 2009]) shows one value that is more depleted than any of our simulations.

[28] Finally, data from intermediate depth in the Indian Ocean is shown in Figures 9a and 9b [*Bryan et al.*, 2010]. All paleo data are more depleted than the corresponding water mass in our simulation.

[29] In summary, there is paleoproxy evidence of at least one depleted deep water mass in the northern North Atlantic (Figures 8a, 8b and 8c) as well as a deep water mass in the Southern Ocean (Figures 9d and 9h) that the model is not able to reproduce. The model also overestimates ventilation rates at intermediate depth in some location in the Atlantic Ocean (Figures 8i and 8j), the Pacific Ocean (Figures 7h and 7k), the Indian Ocean (Figure 9a and b) and the Drake Passage (Figures 9f and 9g). Our equilibrium simulation A-eq is in better agreement with the sparse data available just prior to the start of the Mystery Interval than equilibrium simulation B-eq. During the Mystery Interval no clear

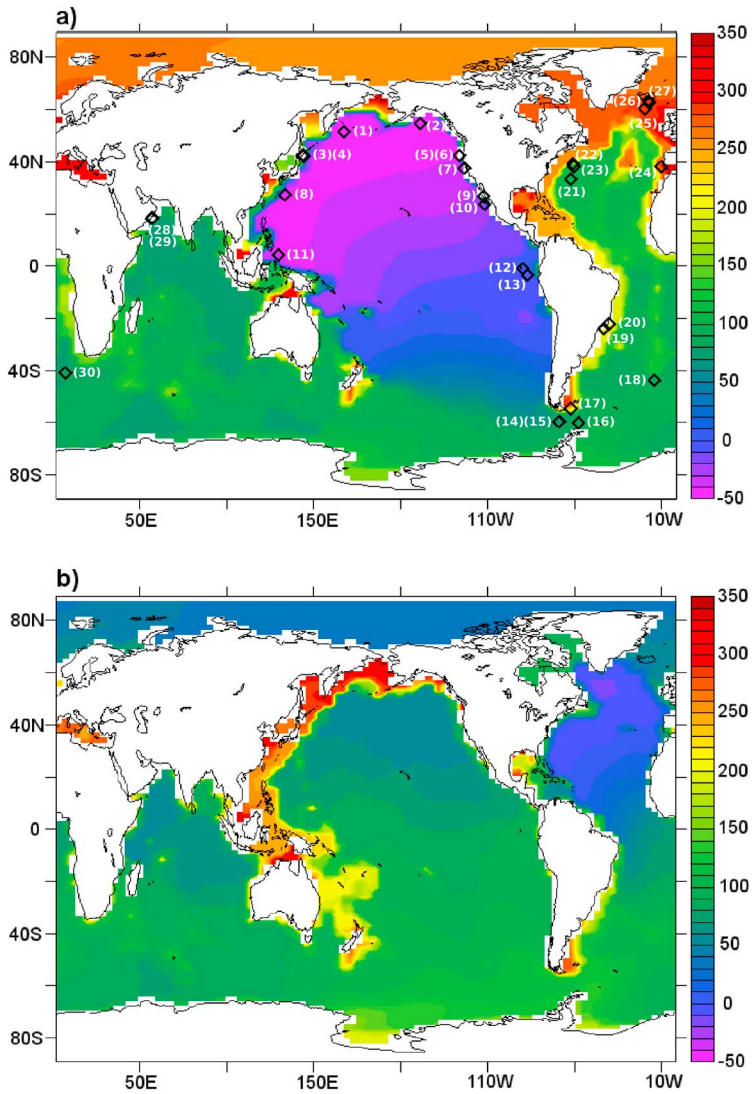

Figure 3. Minimum $\Delta^{14}C$ (permil) in the water column for (a) equilibrium simulation A-eq and (b) equilibrium simulation B-eq. Also shown are the locations of sediment cores and corals discussed in text and shown in Figures 7, 8 and 9. MD01-2416 (1, *Sarnthein et al.* [2006]), ODP-887 (2, *Galbraith et al.* [2007]), GH02-1030 (3, *Ikehara et al.* [2006]), CH84-14 (4, *Duplessy et al.* [1989]), 1019A01H4 (5, *Mix et al.* [1999]) and W8709A-13PC (6, *Mix et al.* [1999]), F8-90-G21 (7, *van Geen et al.* [1996]), KT89-18-P4 (8, *Murayama et al.* [1992]), JPC56 (9, *Keigwin* [2002]), PC08 (10, *Marchitto et al.* [2007]), MD01-2386 (11, *Broecker et al.* [2008]), VM21-30 (12, *Stott et al.* [2009]), TR163-31 (13, *Shackleton et al.* [1988]), 47396B (14, *Goldstein et al.* [2001]), DC-A-2a (15, *Burke and Robinson* [2012]), DC-A-6 (16,*Burke and Robinson* [2012]), DN-A-10 (17, *Burke and Robinson* [2012]), MDO7-3076 (18, *Skinner et al.* [2010]), C2 (19, *Mangini et al.* [2010]), C1 (20, *Mangini et al.* [2010]), Muir1 and Muir2 (21, *Robinson et al.* [2005]), GREGG (22, *Robinson et al.* [2005]), Manning (23, *Robinson et al.* [2005]), MD99-2334K (24, *Skinner and Shackleton* [2004]), RAPiD 17-5P (25, *Thornalley et al.* [2011]), RAPiD 15-4P (26, *Thornalley et al.* [2011]) and RAPiD 10-1P (27, *Thornalley et al.* [2011]), RC2714 (28, *Bryan et al.* [2010]) and RC2723 (29, *Bryan et al.* [2010]) and TNO57-21 (30, *Barker et al.* [2009]).

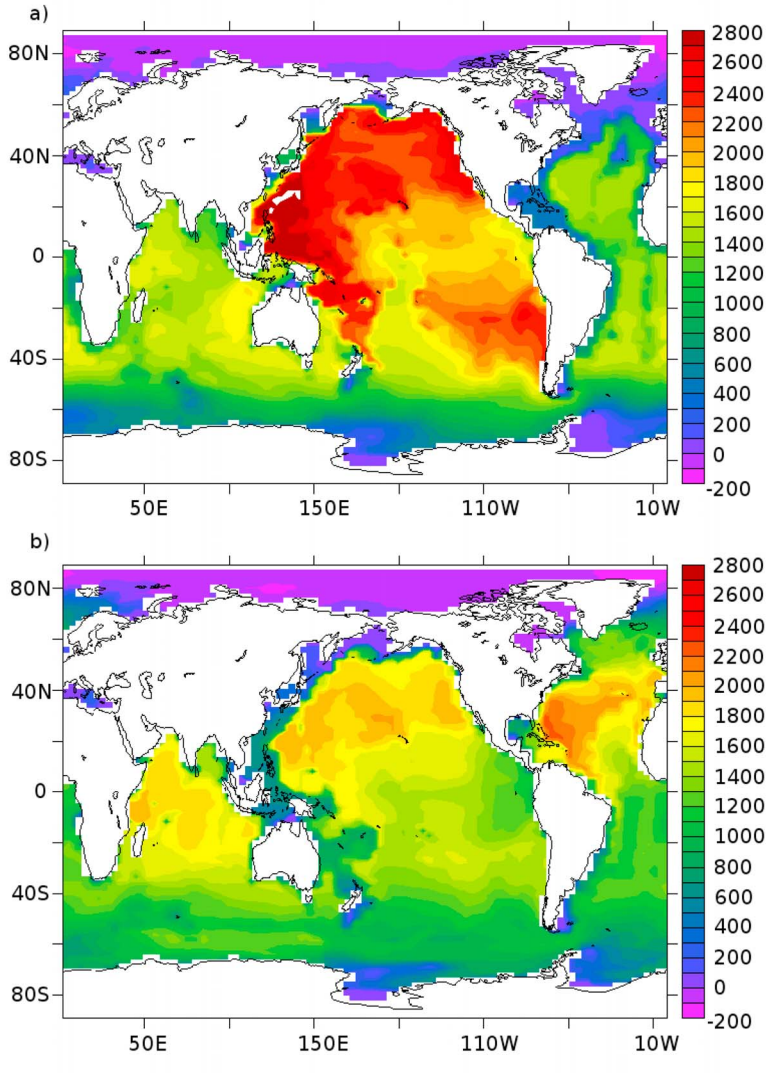

Figure 4. The top - bottom age difference for (a) Simulation A-eq and (b) Simulation B-eq. Units in years.

Table 2. Carbon Anomalies (Sensitivity Simulation Minus Parent Equilibrium Simulation) at Completion of the Simulations[a]

		Ocean						
Simulation	Atmosphere	Total	Deep	Shallow	Land	Atlantic	Pacific	Indian
A-ws	−1.1	5.1	−35.2	40.3	−4.2	−90.8	102.1	−6.2
B-ws	−32.3	126.5	187.1	−60.6	−94.3	−146.6	379.2	−106.1
B-wpd	−18.5	61.4	76.4	−15.0	−43.0	−8.5	114.2	−44.3
A-wpd-fs	35.0	−85.3	−187.7	102.4	49.9	−8.2	−65.5	−11.6
B-wn-fs	21.6	−21.0	−10.2	−10.8	−0.4	−362.7	406.7	−65.0
A-ws-fs	34.0	−79.5	−219.5	140.0	45.0	−26.4	−53.4	0.3
B-ws-fs	7.7	25.7	−18.3	44.0	−33.7	−429.5	502.9	−47.7
B-wpd-fs	5.4	30.9	23.8	7.1	−36.7	−408.9	496.6	−56.8
A-wpd-f	11.6	−57.6	−144.2	86.6	45.7	391.5	−443.7	−5.4
B-wn-f	0.6	1.7	0.8	0.9	−2.6	−0.8	2.6	−0.1
A-ws-f	−6.7	13.7	−19.4	33.1	−7.2	263.2	−187.9	−61.6
B-ws-f	−33.2	126.9	187.4	−60.5	−93.6	−143.4	376.3	−106.0
B-wpd-f	−19.7	64.1	9.8	−15.75	−44.0	−8.4	117.3	−44.8

[a]All units in Pg C.

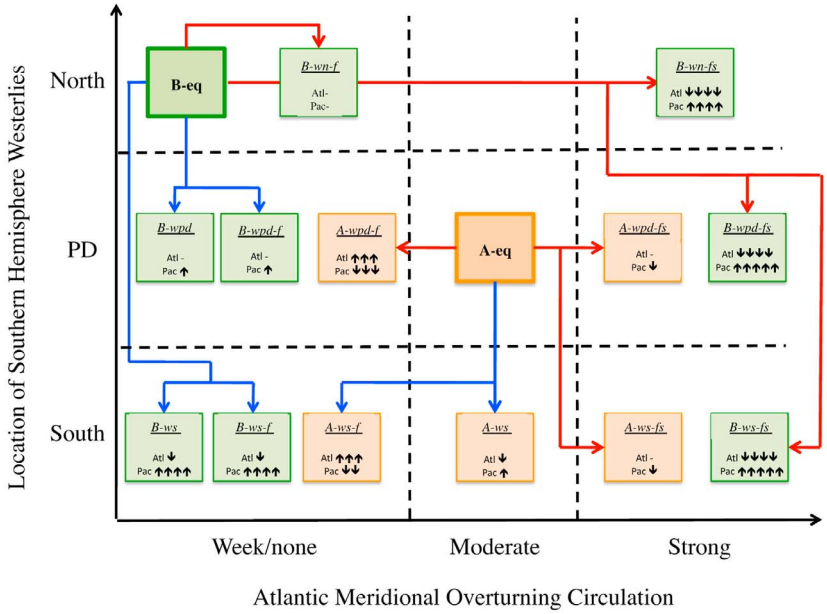

Figure 5. Sensitivity simulations. Atlantic overturning strength (x-axis) versus latitudinal location of SHW (y-axis). 'North' indicates a northward shift by 9° from present-day location, 'PD' indicates present-day location of westerlies, 'South' indicates a southward shift by 9° from present-day location. A and B simulations are colored orange and green respectively. Red arrows indicate a net increase in atmospheric CO_2 while a blue arrow indicates a net decrease in atmospheric CO_2. Each black arrow within a simulation box represents a net increase or decrease of 100 Pg of carbon to the nearest 50 Pg in the Atlantic or Pacific Ocean.

conclusions can be drawn as to which sensitivity study is in best agreement with all available data. Other than for the caveats mentioned above, the model simulations fall within or very close to the error bars of available data.

4. Discussion

4.1. Location of the Mystery Reservoir

[30] While there is no deep water formation in the North Pacific today, *Okazaki et al.* [2010] use a combination of surface proxy data, marine radiocarbon age ventilation records as well as two simulations with LOVECLIM to suggest that deep water was formed in the North Pacific at the beginning of the Mystery Interval. One of our equilibrium simulations (simulation B-eq with SHW shifted 9° north), indeed forms North Pacific Deep Water (NPWD, Figures 1c, 1d and 3b).

[31] When we compare our sensitivity simulations to atmospheric and ocean paleodata, simulations derived from equilibrium simulation A-eq are in better agreement with the data; especially for the atmospheric records (Figure 6) and the ocean records at the start of the interval (Figures 7a and 7h). This is especially important at locations in the northwest Pacific Ocean, where newly ventilated NPDW should have been recorded (cores MD01-2416, GH02-1030, CH 84-14 and KT 89-18-P4; Figures 7a, 7d, 7g and 7j). The two northernmost cores record $\Delta^{14}C$ at or below our simulated values for simulation A-eq. Unless NPDW was located deeper than these cores (situated at 2317 m and 1212 m, respectively), our simulations suggest that there was no significant NPDW formation at the beginning of the Mystery Interval. The deepest cores on the western boundary (KT89-18-P4 at 2700 m and MD01-2386 at 2800 m) are inconclusive when compared to our simulations. While KT89- 18-P4 is in agreement with simulations derived from both equilibrium A-eq and B-eq (Figure 7j), MD01-2386 records younger $\Delta^{14}C$ at the beginning of the interval, closer to our simulated values with active NPDW formation (Figure 7m). One should keep in mind, however, that MD01-2386 is located near the equator, and that coarse resolution ocean models do not resolve equatorial dynamics explicitly well. The four cores along the continental shelf of the western North Atlantic corroborate the data from the northwestern Pacific Ocean (Muir1, Muir2, Manning, Gregg, Figures 8d, 8e, 8f and 8g). All four cores are situated within the flow path of NADW and record a well ventilated water mass close to simulations with active NADW formation. However, none of these records pre-dates the Mystery Interval, so no conclusion can be drawn regarding the circulation before H1.

[32] Therefore, simulation A-eq is a more likely candidate to depict the global circulation just before H1. In simulation A-eq, the oldest carbon-rich water (or 'Mystery Reservoir') is situated in the North Pacific (Figure 3a) in agreement with *Bradtmiller et al.* [2010]. AABW formation is weaker than in simulation B-eq, but still strong enough to keep the Southern Ocean well ventilated. This feature is especially striking when comparing our simulations with the low $\Delta^{14}C$ values recorded by sediment cores TN057-21 and MD07-3076 (Figures 9d and 9h) situated in the South Atlantic at a depth of 4981 m and 3770 m, respectively. These are the only records in the deep ocean in our model-data comparison,

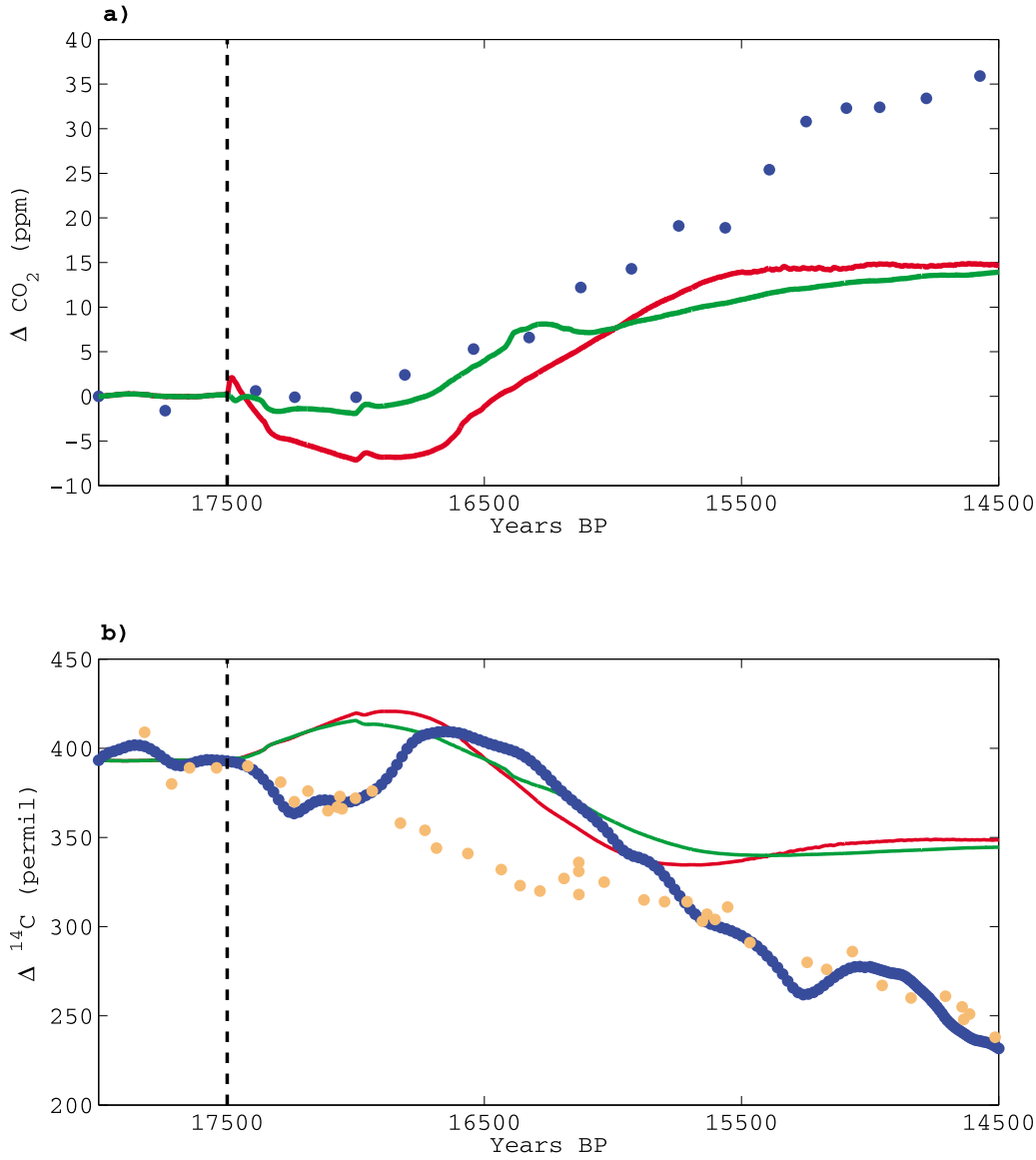

Figure 6. Simulated change in (a) atmospheric CO_2 concentration and (b) total atmospheric $\Delta^{14}C$ for simulations A-ws-fs (red) and A-wpd-fs (green). These are compared to CO_2 data (blue dots) from *Monnin et al.* [2004] on the EDC1 timescale (Figure 6a) as well as $\Delta^{14}C$ data from *Reimer et al.* [2009] (blue dots) and *Southon et al.* [2012] (orange dots, Figure 6b). The black dashed vertical line indicates the start of our sensitivity experiments.

which suggest the existence of a depleted bottom water mass that our simulations are unable to reproduce. The ventilation of the Southern Ocean in all our simulations might therefore be overestimated, and we cannot rule out Southern Ocean waters as a potential 'Mystery Reservoir'. In addition, our simulations overestimate the ventilation at numerous locations at intermediate depth during the interval; and therefore are unable to reconstruct the spread of depleted water masses from the 'Mystery Reservoir' into intermediate depths.

4.2. Ventilation of the Mystery Reservoir

[33] The only mechanism leading to a significant increase in atmospheric CO_2 as well as decrease in $\Delta^{14}C$ in our 13 sensitivity simulations is a strengthening of the AMOC (Figures 5 and 6). Shifting SHW southward leads to a decrease in atmospheric CO_2, unless NADW formation increases simultaneously (Figure 5). This result is puzzling: an increase in NADW formation would also increase heat transport toward the North Atlantic and therefore result in higher temperatures in Europe and Greenland during the interval. However, paleoproxy data suggests a decrease in temperature in Greenland, the North Atlantic and the Mediterranean which lasted for the entire Mystery Interval [*Bard et al.*, 2000; *Stuiver and Grootes*, 2000; *Broecker and Barker*, 2007; *Moreno et al.*, 2010]. On the other hand, in the subantarctic Pacific, there is evidence for an increase in SST with a noticeable drop occurring around the time of the Bølling-Allerød/Antarctic Cold Reversal (B-A/ACR) [*Kiefer and Kienast*, 2005]. Antarctica warmed more rapidly than the Northern Hemisphere, during H1 we see a recession of

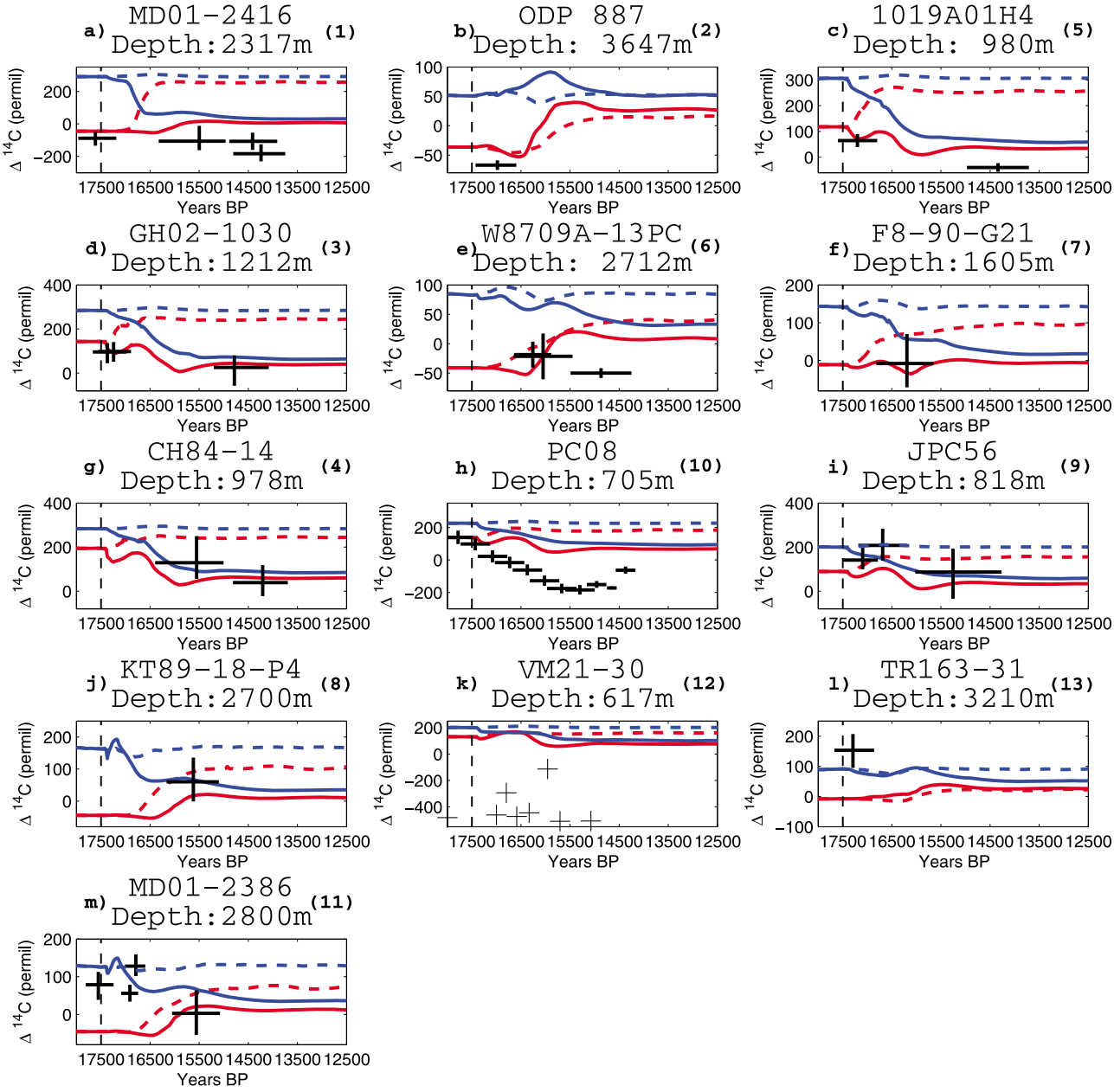

Figure 7. Pacific Ocean: Simulated $\Delta^{14}C$ values for A-wpd-f (red dashed), A-ws-fs (red solid), B-wn-f (blue dashed) and B-ws-fs (blue solid) compared to proxy data (black crosses). The black dashed vertical line indicates the start of our sensitivity experiments while the numbers next to each core name refer to Figure 3a. Shown are data from cores: (a) MD01-2416 [*Sarnthein et al.*, 2006], (b) ODP-887 [*Galbraith et al.*, 2007], (c) 1019A01H4 [*Mix et al.*, 1999], (d) GH02-1030 [*Ikehara et al.*, 2006], (e) W8709A-13PC [*Mix et al.*, 1999], (f) F8-90-G21 [*van Geen et al.*, 1996], (g) CH84-14 [*Duplessy et al.*, 1989], (h) PC08 [*Marchitto et al.*, 2007], (i) JPC56 [*Keigwin*, 2002], (j) KT89-18-P4 [*Murayama et al.*, 1992], (k) VM21-30 [*Stott et al.*, 2009; *Stott and Timmermann*, 2011], (l) TR163-31 [*Shackleton et al.*, 1988] and (m) MD01-2386 [*Broecker et al.*, 2008]. It should be noted that VM21-30 (Figure 7k) is shown without error bars.

Antarctic sea ice and increased SST, particularly in the area of the sub-tropical front [*Denton et al.*, 2010]. An increased ventilation of the Southern Ocean as a result of a weakened AMOC would therefore be in better agreement with most of the paleodata [*Meissner et al.*, 2008].

[34] None of our simulations show this mechanism. One possible reason is that the seesaw between Northern and Southern Hemisphere [e.g., *Broecker*, 1998; *Stocker*, 1998; *Stocker and Johnsen*, 2003; *Sigman et al.*, 2007] in our model is attenuated by the existence of a Pacific-Atlantic see-saw [*Okazaki et al.*, 2010; *Saenko et al.*, 2004]; i.e. when NADW formation is weakened, NPDW formation switches on under H1 boundary conditions and therefore AAWB and AAIW formation rates are not as strong as they would be

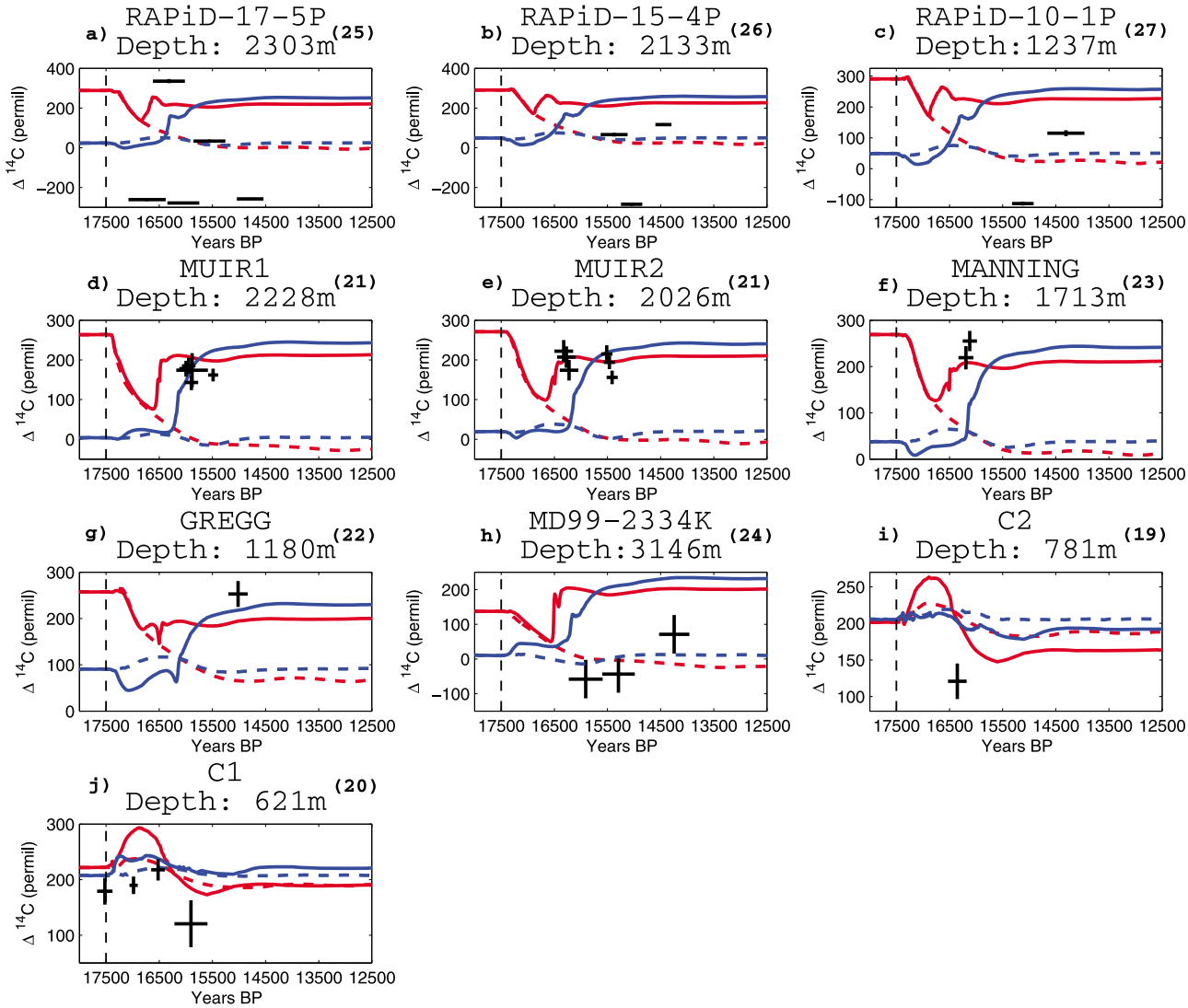

Figure 8. Atlantic Ocean: Simulated $\Delta^{14}C$ values for A-wpd-f (red dashed), A-ws-fs (red solid), B-wn-f (blue dashed) and B-ws-fs (blue solid) compared to proxy data (black crosses). The black dashed vertical line indicates the start of our sensitivity experiments while the numbers next to each core name refer to Figure 3a. Shown are data from cores (a) RAPiD 17-5P [*Thornalley et al.*, 2011], (b) RAPiD 15-4P [*Thornalley et al.*, 2011], (c) RAPiD 10-1P [*Thornalley et al.*, 2011], (d) MUIR1 [*Robinson et al.*, 2005], (e) MUIR2 [*Robinson et al.*, 2005], (f) MANNING [*Robinson et al.*, 2005], (g) GREGG [*Robinson et al.*, 2005], (h) MD99-2334K [*Skinner and Shackleton*, 2004] and coral records (i) C2 [*Mangini et al.*, 2010] and (j) C1 [*Mangini et al.*, 2010]. It should be noted that MUIR2 contains data from two different depths (2026 m and 2084 m) which correspond to the same interpolated depth in our model and were therefore plotted on a single figure.

without North Pacific ventilation. Another caveat might be the design of our sensitivity studies; it is likely that there were important mechanisms at play other than shifted SHW and changes in AMOC. For example, *d'Orgeville et al.* [2010] show that changes in the strength of SHW are more significant in altering atmospheric CO_2 than changes in the location of SHW. On the other hand, not all data agrees with the simplified picture of simultaneous northern hemispheric cooling and southern hemispheric warming during the Mystery Interval. For example, *Rühlemann et al.* [1999] report warming in the western low-latitude Atlantic during the H1 event based on alkenone reconstructions. *Kiefer and Kienast* [2005] used SST proxies of Mg/Ca ratios, foraminiferal assemblages and alkenone saturation reconstructions to create a clearer picture of SST during the deglaciation. Their results show a continuous warming throughout the deglaciation beginning at 19 $\pm$ 1 ka BP. Furthermore, they show that half the deglacial warming occurred prior to the onset of the Bølling warming and that there is no clear indication of a cessation of global SST increase during H1, B-A, Antarctic Cold Reversal (ACR) at 14.5 ka BP or the YD. The reader should also keep in mind that the AMOC response to freshwater hosing as well as the subsequent

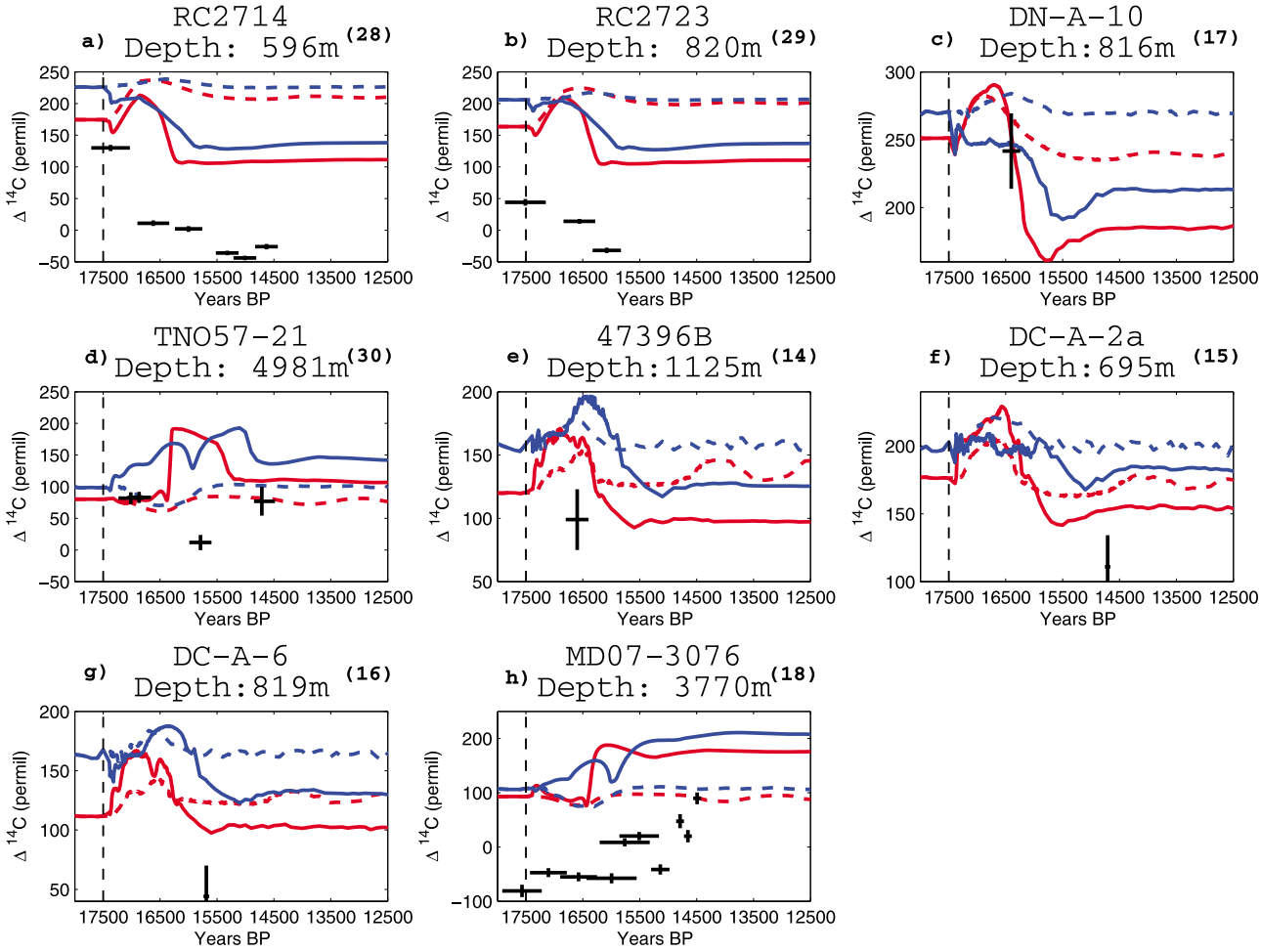

Figure 9. Southern and Indian Ocean: Simulated $\Delta^{14}C$ values for A-wpd-f (red dashed), A-ws-fs (red solid), B-wn-f (blue dashed) and B-ws-fs (blue solid) compared to proxy data (black crosses or horizontal segments). The black dashed vertical line indicates the start of our sensitivity experiments while the numbers next to each core name refer to Figure 3a. Shown are data from cores (a) RC2714 [*Bryan et al.*, 2010], (b) RC2723 [*Bryan et al.*, 2010], (c) deep sea coral DN-A-10 [*Burke and Robinson*, 2012], (d) sediment core TNO57-21 [*Barker et al.*, 2009], (e) deep sea coral 47396B [*Goldstein et al.*, 2001], (f) deep sea corals DC-A-2a [*Burke and Robinson*, 2012] and (g) DC-A-6 [*Burke and Robinson*, 2012] and (h) sediment core MDO7-3076 [*Skinner et al.*, 2010].

changes in carbon budgets are model dependent [*Bouttes et al.*, 2012].

[35] Figure 10a shows that despite the large amount of $\Delta^{14}C$ depleted water in the North Pacific Ocean in simulation A-eq, the largest change in ocean $\Delta^{14}C$ values occurs in the Atlantic basin during the transient simulation A-ws-fs, with comparatively little of the Pacific old water being ventilated. Simulation A-wpd-fs shows similar results with the Atlantic being the main source for ventilated carbon (not shown). While the location of the SHW has virtually no effect on the amount of ^{14}C ventilated in the Atlantic, a southward wind shift leads to a higher ventilation of the Pacific Ocean and lower ventilation of the Southern Ocean (Figure 10b). It should be noted that these figures only indicate changes in averaged $\Delta^{14}C$ over the water column, these changes imply ventilation as well as redistribution of carbon within in the ocean.

[36] Finally, some of our sensitivity simulations show large exchanges of carbon between the Atlantic and Pacific basin (Figure 5), in some cases exceeding 400 Pg C (or an equivalent of 200 ppm). This is a result of a shift in deep water formation sites between the North Atlantic and North Pacific. Very little of this 'transferred' carbon makes it into the atmosphere.

5. Conclusions

[37] We use the UVic Earth System Climate Model (UVic ESCM) under Heinrich Event 1 (H1) boundary conditions in an attempt to (i) locate the oldest water masses in the ocean ('Mystery Reservoir') and (ii) test the ability of two mechanisms, namely, the strength of the Atlantic Meridional Overturning Circulation (AMOC) and latitudinal shifts of Southern Hemisphere Westerlies (SHW), to ventilate this carbon rich, ^{14}C deficient ocean reservoir. The UVic ESCM equilibrates with a moderate AMOC when forced with a combination of H1 boundary conditions and present-day winds; in this simulation the oldest water masses are found

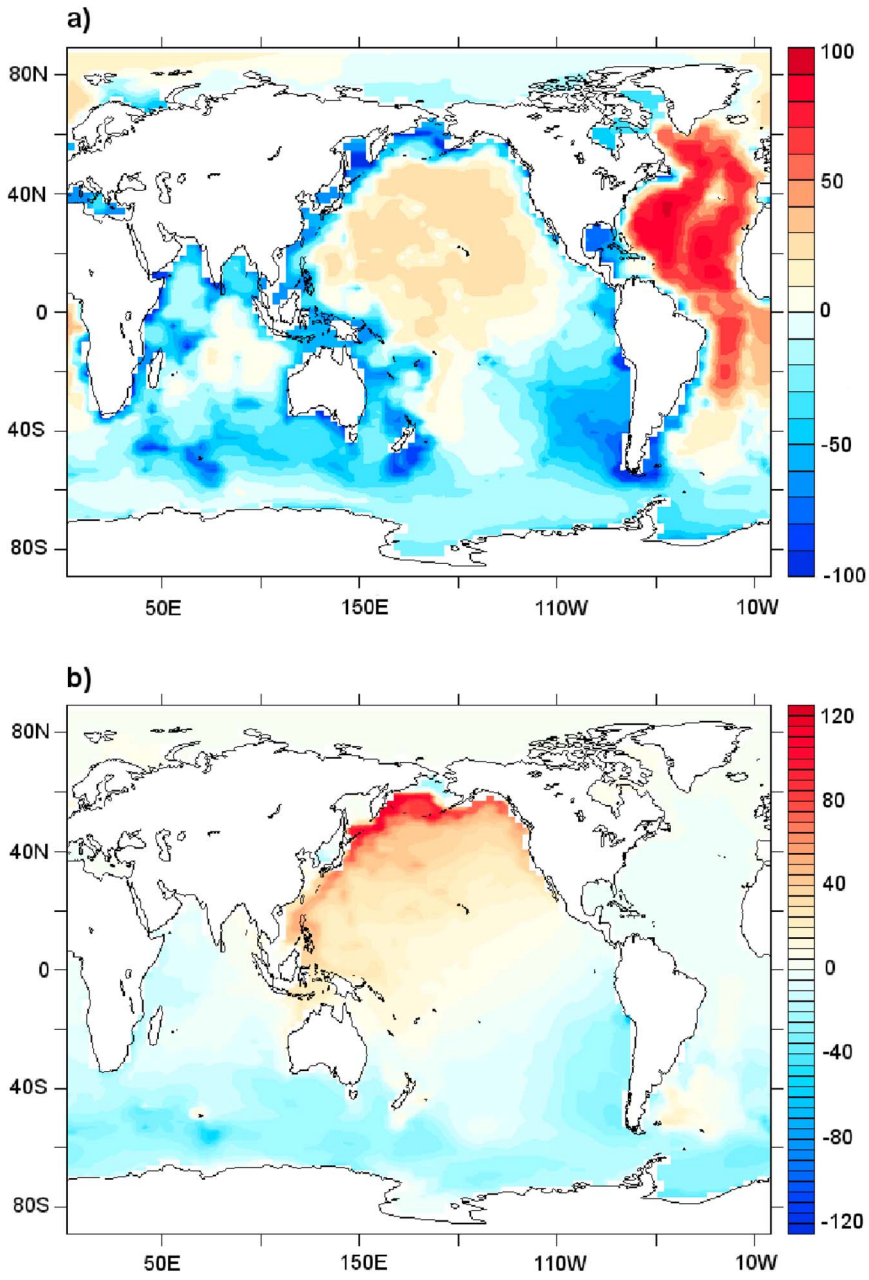

Figure 10. $\Delta^{14}C$ anomalies (permil) during simulations A-ws-fs and A-wpd-fs. (a) Difference between conditions at the end of the simulation and conditions before the restart of the AMOC (simulation A-ws-fs). (b) Difference of $\Delta^{14}C$ anomalies (A-ws-fs minus A-wpd-fs). $\Delta^{14}C$ values are averaged over the entire water column.

in the North Pacific Ocean similar to present-day conditions. When forced with a combination of H1 boundary conditions and northward shifted SHW, the model establishes a strong Pacific Meridional Overturning Circulation (PMOC) with oldest water masses found in the North Atlantic in agreement with *Okazaki et al.* [2010]. None of our equilibrium simulations produces very old water in the Southern Ocean.

[38] We subsequently conduct 13 sensitivity studies based on these two equilibrium simulations by shifting SHW southward and altering the strength of the AMOC. We find that neither a southward shift in SHW, nor the shut-down and subsequent strengthening of NH overturning or any combination of the two can account for the entire reconstructed increase in atmospheric CO_2 or decrease in atmospheric $\Delta^{14}C$ during the Mystery Interval. Shifting SHW south results in a decrease in atmospheric CO_2 and a massive reorganisation of deep ocean carbon budgets, predominately between the Pacific and Atlantic Basins while little of this ventilates. Weakening the AMOC and subsequently re-starting it results in significant increases in atmospheric

CO_2 and a reduction in atmospheric $\Delta^{14}C$. Whenever the two mechanisms are combined, the strength of the AMOC is the dominant mechanism resulting in an increase in atmospheric CO_2.

[39] While perturbations of the AMOC are the dominant forcing mechanism, the simulation in which both SHW are shifted south and in which the AMOC is weakened then strengthened provides the closest results to reconstructed CO_2 and $\Delta^{14}C$ records. It can account for 58% of the observed atmospheric CO_2 increase and 45% of the atmospheric $\Delta^{14}C$ decrease. The rate of change is similar to reconstructions, but the ventilation cannot be sustained to account for the entire change. However, this mechanism of ventilation is unlikely as it would have resulted in a warming of the Northern Hemisphere during the Mystery Interval, which is in conflict with available paleodata. It should also be noted that a significant part of the decline in atmospheric $\Delta^{14}C$ could be due to changes in the ^{14}C production rate [*Köhler et al.*, 2006]. The terrestrial carbon plays a non-negligible role in the uptake of ventilated ocean carbon, always gaining more than the atmosphere.

[40] When comparing our simulations to paleodata, we find that simulations forming deep water in the North Atlantic before the onset of the Mystery Interval are in better agreement than simulations forming deep water in the North Pacific. None of our simulations forms or ventilates old water masses in/from the Southern Ocean. This might be due to the fact that the north-south seesaw is attenuated by the existence of a Pacific-Atlantic seesaw in our model. As a consequence, our model is not able to reproduce old water masses recorded in several locations at intermediate depths later in the interval and is also likely to underestimate the drop in atmospheric $\Delta^{14}C$.

[41] **Acknowledgments.** We would like to thank two anonymous reviewers for their very valuable comments, suggestions and help. This work was supported by the Australian Research Council Future Fellowship program (FT100100443). W.N.H. is thankful for an Honors student scholarship by the ARC Centre of Excellence for Climate System Science. We are grateful for an award under the Merit Allocation Scheme on the NCI National Facility at the ANU.

References

Adkins, J. F., K. McIntyre, and D. P. Schrag (2002), The salinity, temperature, and $\delta^{18}O$ of the glacial deep ocean, *Science*, *298*(5599), 1769–1773.

Anderson, R. F., and M.-E. Carr (2010), Uncorking the Southern Ocean's vintage CO_2, *Science*, *328*(5982), 1117–1118.

Anderson, R., S. Ali, L. I. Bradtmiller, S. H. H. Nielsen, M. Q. Fleisher, B. E. Anderson, and L. H. Burckle (2009), Wind-driven upwelling in the Southern Ocean and the deglacial rise in atmospheric CO_2, *Science*, *323*, 1443–1448.

Archer, D. (1996), A data-driven model of the global calcite lysocline, *Global Biogeochem. Cycles*, *10*(3), 511–526.

Bard, E., F. Rostek, J.-L. Turon, and S. Gendreau (2000), Hydrological impact of Heinrich Events in the subtropical Northeast Atlantic, *Science*, *289*(5483), 1321–1323.

Barker, S., P. Diz, M. J. Vautravers, J. Pike, G. Knorr, I. R. Hall, and W. S. Broecker (2009), Interhemispheric Atlantic seesaw response during the last deglaciation, *Nature*, *457*(7233), 1097–1102.

Basak, C., E. E. Martin, K. Horikawa, and T. M. Marchitto (2010), Southern Ocean source of ^{14}C-depleted carbon in the North Pacific Ocean during the last deglaciation, *Nat. Geosci.*, *3*(11), 770–773.

Berger, A. L. (1978), Long-term variations of daily insolation and quaternary climatic changes, *J. Atmos. Sci.*, *35*, 2362–2367.

Bouttes, N., D. M. Roche, and D. Paillard (2012), Systematic study of the impact of fresh water fluxes on the glacial carbon cycle, *Clim. Past*, *8*, 589–607.

Bradtmiller, L. I., R. F. Anderson, J. P. Sachs, and M. Q. Fleisher (2010), A deeper respired carbon pool in the glacial equatorial Pacific Ocean, *Earth Planet. Sci. Lett.*, *299*, 417–425.

Broecker, W. S. (1998), Paleocean circulation during the last deglaciation: A bipolar see-saw?, *Paleoceanography*, *13*, 1862–1864.

Broecker, W. (2009), The mysterious ^{14}C decline, *Radiocarbon*, *51*(1), 109–119.

Broecker, W., and S. Barker (2007), A 190‰ drop in atmosphere's $\Delta^{14}C$ during the 'Mystery Interval' (17.5 to 14.5 kyr), *Earth Planet. Sci. Lett.*, *256*(1–2), 90–99.

Broecker, W., and E. Clark (2010), Search for a glacial-age ^{14}C-depleted ocean reservoir, *Geophys. Res. Lett.*, *37*, L13606, doi:10.1029/2010GL043969.

Broecker, W., E. Clark, and S. Barker (2008), Near constancy of the Pacific Ocean surface to mid-depth radiocarbon-age difference over the last 20 kyr, *Earth Planet. Sci. Lett.*, *274*(3–4), 322–326.

Brook, E. (2012), The ice age carbon puzzle, *Science*, *336*, 682–683.

Bryan, S. P., T. M. Marchitto, and S. J. Lehman (2010), The release of ^{14}C-depleted carbon from the deep ocean during the last deglaciation: Evidence from the Arabian Sea, *Earth Planet. Sci. Lett.*, *298*(1–2), 244–254.

Burke, A., and L. Robinson (2012), The Southern Oceans role in carbon exchange during the last deglaciation, *Science*, *335*(6068), 557–562.

Cheng, H., R. L. Edwards, W. S. Broecker, G. H. Denton, X. Kong, Y. Wang, R. Zhang, and X. Wang (2009), Ice age terminations, *Science*, *326*(5950), 248–252.

Chiang, J. (2009), The tropics in Paleoclimate, *Annu. Rev. Earth Planet Sci.*, *37*, 263–297.

Clark, P. U., A. S. Dyke, J. D. Shakun, A. E. Carlson, J. Clark, B. Wohlfarth, J. X. Mitrovica, S. W. Hostetler, and A. M. McCabe (2009), The Last Glacial Maximum, *Science*, *325*, 710–714.

Clark, P. U., et al. (2012), Global climate evolution during the last deglaciation, *Proc. Natl. Acad. Sci. U. S. A.*, *109*(19), E1134–E1142.

Denton, G. H., R. F. Anderson, J. R. Toggweiler, R. L. Edwards, J. M. Schaefer, and A. E. Putnam (2010), The Last Glacial Termination, *Science*, *328*(5986), 1652–1656.

De Pol-Holz, R., L. Keigwin, J. Southon, D. Hebbeln, and M. Mohtadi (2010), No signature of abyssal carbon in intermediate waters off Chile during deglaciation, *Nat. Geosci.*, *3*, 192–195.

d'Orgeville, M., W. P. Sijp, M. H. England, and K. J. Meissner (2010), On the control of glacial-interglacial atmospheric CO_2 variations by the Southern Hemisphere westerlies, *Geophys. Res. Lett.*, *37*, L21703, doi:10.1029/2010GL045261.

Duplessy, J. C., M. Arnold, E. Bard, A. Juillet-Leclerc, N. Kalleb, and L. Labeyrie (1989), AMS ^{14}C study of transient events and of the ventilation rate of the Pacific intermediate water during the last deglaciation, *Radiocarbon*, *31*, 493–502.

Galbraith, E. D., S. L. Jaccard, T. F. Pedersen, D. M. Sigman, G. H. Haug, M. Cook, J. R. Southon, and R. Francois (2007), Carbon dioxide release from the North Pacific abyss during the last deglaciation, *Nature*, *449*, 890–893.

Gersonde, R., et al. (2003), Last glacial sea surface temperatures and sea-ice extent in the Southern Ocean (Atlantic-Indian sector): A multiproxy approach, *Paleoceanography*, *18*(3), 1061, doi:10.1029/2002PA000809.

Goldstein, S. J., D. W. Lea, S. Chakraborty, M. Kashgarian, and M. Murrell (2001), Uranium-series and radiocarbon geochronology of deep-sea corals: Implications for Southern Ocean ventilation rates and the oceanic carbon cycle, *Earth Planet. Sci. Lett.*, *193*, 167–182.

Grootes, P. M., M. Stuiver, J. W. C. White, S. J. Johnsen, and J. Jouzel (1993), Comparison of oxygen isotope records from the GISP2 and GRIP Greenland ice cores, *Nature*, *366*, 552–554.

Hain, M. P., D. M. Sigman, and G. H. Haug (2011), Shortcomings of the isolated abyssal reservoir model for deglacial radiocarbon changes in the mid-depth Indo-Pacific Ocean, *Geophys. Res. Lett.*, *38*, L04604, doi:10.1029/2010GL046158.

Hemming, S. R. (2004), Heinrich events: Massive late Pleistocene detritus layers of the North Atlantic and their global climate imprint, *Rev. Geophys.*, *42*, RG1005, doi:10.1029/2003RG000128.

Hesse, P. P. (1994), The record of continental dust from Australia in Tasman sea sediments, *Quat. Sci. Rev.*, *13*(3), 257–272.

Hibler, W. D., III (1979), A dynamic thermodynamic sea ice model, *J. Phys. Oceanogr.*, *9*(4), 815–846.

Hunke, E. C., and J. K. Dukowicz (1997), An elastic-viscous-plastic model for sea ice dynamics, *J. Phys. Oceanogr.*, *27*(9), 1849–1867.

Ikehara, K., K. Ohkushi, A. Shibahara, and M. Hoshiba (2006), Change of bottom water conditions at intermediate depths of the Oyashio region, NW Pacific over the past 20,000 yrs, *Global Planet. Change*, *53*, 78–91.

Kalnay, E., et al. (1996), The NCEP/NCAR 40-year reanalysis project, *Bull. Am. Meteorol. Soc.*, *77*(3), 437–471.

Keigwin, L. D. (2002), Late Pleistocene-Holocene paleoceanography and ventilation of the Gulf of California, *J. Oceanogr.*, *58*(2), 421–432.

Kiefer, T., and M. Kienast (2005), Patterns of deglacial warming in the Pacific Ocean: A review with emphasis on the time interval of Heinrich event 1, *Quat. Sci. Rev.*, *24*(7–9), 1063–1081.

Köhler, P., R. Muscheler, and H. Fischer (2006), A model-based interpretation of low-frequency changes in the carbon cycle during the last 120,000 years and its implications for the reconstruction of atmospheric $\Delta^{14}C$, *Geochem. Geophys. Geosyst.*, *7*, Q11N06, doi:10.1029/2005GC001228.

Kovaltsov, G., A. Mishev, and I. G. Usoskin (2012), A new model of cosmogenic production of radiocarbon ^{14}C in the atmosphere, *Earth Planet. Sci. Lett.*, *337–338*, 114–120.

Lamy, F., D. Hebbeln, and G. Wefer (1999), High-resolution marine record of climatic change in mid-latitude Chile during the last 28,000 years based on terrigenous sediment parameters, *Quat. Res.*, *51*(1), 83–93.

Liu, Z., et al. (2009), Transient simulation of last deglaciation with a new mechanism for Bølling-Allerød warming, *Science*, *325*(1989), 310–314.

Lund, D. C., A. C. Mix, and J. Southon (2011), Increased ventilation age of the deep northeast Pacific Ocean during the last deglaciation, *Nat. Geosci.*, *4*, 771–774.

Mangini, A., J. M. Godoy, M. L. Godoy, R. Kowsmann, G. M. Santos, M. Ruckelshausen, A. Schroeder-Ritzrau, and L. Wacker (2010), Deep sea corals off Brazil verify a poorly ventilated Southern Pacific Ocean during H2, H1 and the Younger Dryas, *Earth Planet. Sci. Lett.*, *293*(3–4), 269–276.

Marchitto, T. M., S. J. Lehman, J. D. Ortiz, J. Flückiger, and A. Van Geen (2007), Marine radiocarbon evidence for the mechanism of deglacial atmospheric CO_2 rise, *Science*, *316*(5830), 1456–1459.

McGlone, M. S., C. S. M. Turney, J. M. Wilmshurst, J. Renwick, and K. Pahnke (2010), Divergent trends in land and ocean temperature in the Southern Ocean over the past 18,000 years, *Nat. Geosci.*, *3*, 622–626.

McManus, J. F., R. Francois, J.-M. Gherardi, L.-D. Keigwin, and S. Brown-Leger (2004), Collapse and rapid resumption of Atlantic meridional circulation linked to deglacial climate changes, *Nature*, *428*(6985), 834–837.

Meissner, K. J. (2007), Younger Dryas: A data to model comparison to constrain the strength of the overturning circulation, *Geophys. Res. Lett.*, *34*, L21705, doi:10.1029/2007GL031304.

Meissner, K. J., A. J. Weaver, H. D. Matthews, and P. M. Cox (2003a), The role of land surface dynamics in glacial inception: A study with the UVic Earth System Model, *Clim. Dyn.*, *21*, 515–537.

Meissner, K. J., A. Schmittner, A. J. Weaver, and J. F. Adkins (2003b), Ventilation of the North Atlantic Ocean during the Last Glacial Maximum: A comparison between simulated and observed radiocarbon ages, *Paleoceanography*, *18*(2), 1023, doi:10.1029/2002PA000762.

Meissner, K. J., M. Eby, A. J. Weaver, and O. Saenko (2008), CO_2 threshold for millennial-scale oscillations in the climate system: Implications for global warming scenarios, *Clim. Dyn.*, *30*, 161–174.

Mix, A. C., D. C. Lund, N. G. Pisias, P. Bodén, L. Bornmalm, M. Lyle, and J. Pike (1999), Rapid climate oscillations in the northeast Pacific during the last deglaciation reflect Northern and Southern Hemisphere sources, in *Mechanisms of Global Climate Change at Millennial Time Scales*, *Geophys. Monogr. Ser.*, vol. 112, edited by U. Clark, S. Webb, and D. Keigwin, pp. 127–148, AGU, Washington, D. C.

Monnin, E., A. Indermühle, A. Dällenbach, J. Flückinger, B. Stauffer, T. F. Stocker, D. Raynaud, and J.-M. Barnola (2001), Atmospheric CO_2 concentrations over the Last Glacial Termination, *Science*, *291*, 112–114.

Monnin, E., et al. (2004), EPICA Dome C ice core high resolution Holocene and transition CO_2 data, http://gcmd.nasa.gov/KeywordSearch/Metadata.do?Portal=GCMD&KeywordPath=Parameters|PALEOCLIMATE|ICE+CORE+RECORDS|CARBON+DIOXIDE&EntryId=PALEO_EPICA_2004-055&MetadataView=Full&MetadataType=0&lbnode=mdlb3, World Data Cent. for Paleoclimatol., Boulder, Colo.

Moreno, A., H. Stoll, M. Jiménez-Sànchez, I. Cacho, B. Valero-Garcés, E. Ito, and R. L. Edwards (2010), A speleothem record of glacial (25–11.6 kyr BP) rapid climatic changes from northern Iberian Peninsula, *Global Planet. Change*, *71*(3–4), 218–231.

Moreno, P. I., T. V. Lowell, G. L. Jacobson Jr., and G. H. Denton (1999), Abrupt vegetation and climate changes during the Last Glacial Maximum and Last Termination in the Chilean lake district: A case study from Canal de la Puntilla (41°S), *Quat. Sci. Rev.*, *81*(2), 285–311.

Morgan, V., M. Delmotte, T. van Ommen, J. Jouzel, J. Chappellaz, S. Woon, V. Masson-Delmotte, and D. Raynaud (2002), Relative timing of deglacial climate events in Antarctica and Greenland, *Science*, *297*(5588), 1862–1864.

Murayama, M., A. Taira, H. Iwakura, E. Matsumoto, and T. Nakamura (1992), Northwest Pacific deep water ventilation rate during the past 35,000 years with the AMS ^{14}C foraminifera ages, *Summ. Res. Using AMS Nagoya Univ.*, *3*, 114–121.

Okazaki, Y., A. Timmermann, L. Menviel, N. Harada, A. Abe-Ouchi, M. O. Chikamoto, A. Mouchet, and H. Asahi (2010), Deepwater formation in the North Pacific during the Last Glacial Termination, *Science*, *329*(5988), 200–204.

Pacanowski, R. C. (1995), MOM 2 documentation, user's guide and reference manual, *Tech. Rep. 3*, GFDL Ocean Group, Geophys. Fluid Dyn. Lab., Princeton, N. J.

Pahnke, K., S. L. Goldstein, and S. R. Hemming (2008), Abrupt changes in Antarctic Intermediate Water circulation over the past 25,000 years, *Nat. Geosci.*, *1*, 870–874.

Peltier, W. R. (2002), Global glacial isostatic adjustment: Palaeogeodetic and space-geodetic tests of the ICE-4G (VM2) model, *J. Quat. Sci.*, *17*(5–6), 491–510.

Peterson, L., G. Haug, K. A. Hughen, and U. Röhl (2000), Rapid changes in the hydrologic cycle of the tropical Atlantic during the Last Glacial, *Science*, *290*, 1947–1951.

Reimer, P. J., et al. (2009), Intcal09 and Marine09 radiocarbon age calibration curves, 0-50,000 years cal BP, *Radiocarbon*, *51*(4), 1111–1150.

Robinson, L. F., J. F. Adkins, L. D. Keigwin, J. Southon, D. P. Fernandez, S.-L. Wang, and D. S. Scheirer (2005), Radiocarbon variability in the western North Atlantic during the last deglaciation, *Science*, *310*(5753), 1469–1473.

Rojas, M., P. Moreno, M. Kageyama, M. Crucifix, C. Hewitt, A. Abe-Ouchi, R. Ohgaito, E. C. Brady, and P. Hope (2009), The Southern Westerlies during the Last Glacial Maximum in PMIP2 simulations, *Quat. Sci. Rev.*, *32*(4), 525–548.

Rose, K. A., E. L. Sikes, T. P. Guilderson, P. Shane, T. M. Hill, R. Zahn, and H. J. Spero (2010), Upper-ocean-to-atmosphere radiocarbon offsets imply fast deglacial carbon dioxide release, *Nature*, *466*(7310), 1093–1097.

Rühlemann, C., S. Mulitza, P. Müller, G. Wefer, and R. Zahn (1999), Warming of the tropical Atlantic Ocean and slowdown of thermohaline circulation during the last deglaciation, *Nature*, *402*, 511–514.

Saenko, O. A., A. J. Weaver, and J. M. Gregory (2003), On the link between the two modes of the ocean thermohaline circulation and the formation of global-scale water masses, *J. Clim.*, *16*(17), 2797–2801.

Saenko, O. A., A. Schmittner, and A. J. Weaver (2004), The Atlantic-Pacific seesaw, *J. Clim.*, *17*(11), 2033–2038.

Sarnthein, M., T. Kiefer, P. M. Grootes, H. Elderfield, and H. Erlenkeuser (2006), Warmings in the far northwestern Pacific promoted pre-Clovis immigration to America during Heinrich event 1, *Geology*, *34*, 141–144.

Schartau, M., and A. Oschlies (2003), Simultaneous data-based optimization of a 1D-ecosystem model at three locations in the North Atlantic Ocean: Part 2. Standing stocks and nitrogen fluxes, *J. Mar. Res.*, *61*(6), 795–821.

Schmitt, J., et al. (2012), Carbon isotope constraints on the deglacial CO_2 rise from ice cores, *Science*, *336*, 711–714.

Schmittner, A., O. A. Saenko, and A. J. Weaver (2003), Coupling of the hemispheres in observations and simulations of glacial climate change, *Quat. Sci. Rev.*, *22*, 659–671.

Schmittner, A., A. Oschlies, H. D. Matthews, and E. D. Galbraith (2008), Future changes in climate, ocean circulation, ecosystems, and biogeochemical cycling simulated for a business-as-usual CO_2 emission scenario until year 4000 AD, *Global Biogeochem. Cycles*, *22*, GB1013, doi:10.1029/2007GB002953.

Semtner, A. J. J. (1976), A model for the thermodynamic growth of sea ice in numerical investigations of climate, *J. Phys. Oceanogr.*, *6*(3), 379–389.

Shackleton, N., J.-C. Duplessy, M. Arnold, P. Maurice, M. Hall, and J. Cartlidge (1988), Radiocarbon age of last glacial Pacific deep water, *Nature*, *335*, 708–711.

Sigman, D. M., A. M. de Boer, and G. H. Haug (2007), Antarctic stratification, atmospheric water vapour, and Heinrich Events: A hypothesis for Late Pleistocene deglaciations, in *Ocean Circulation: Mechanisms and Impacts*, *Geophys. Monogr. Ser.*, vol. 173, edited by A. Schmittner, J. C. H. Chiang, and S. R. Hemming, pp. 335–349, AGU, Washington, D. C.

Skinner, L. C., and N. J. Shackleton (2004), Rapid transient changes in northeast Atlantic deep water ventilation age across Termination I, *Paleoceanography*, *19*, PA2005, doi:10.1029/2003PA000983.

Skinner, L. C., S. Fallon, C. Waelbroeck, E. Michel, and S. Barker (2010), Ventilation of the deep Southern Ocean and deglacial CO_2 rise, *Science*, *328*(5982), 1147–1151.

Smith, H. J., H. Fischer, M. Wahlen, D. Mastroianni, and B. Deck (1999), Dual modes of the carbon cycle since the Last Glacial Maximum, *Nature*, *400*(6741), 248–250.

Southon, J., A. L. Noronha, H. Cheng, R. L. Edwards, and Y. Wang (2012), A high-resolution record of atmospheric ^{14}C based on Hulu Cave speleothem h82, *Quat. Sci. Rev.*, *33*, 32–41.

Stephens, B. B., and R. F. Keeling (2000), The influence of Antarctic sea ice on glacial-interglacial CO_2 variations, *Nature*, *404*, 171–174.

Stocker, T. (1998), The seesaw effect, *Science*, *282*(5386), 61–62.

Stocker, T., and S. Johnsen (2003), A minimum thermodynamic model for the bipolar seesaw, *Paleoceanography*, *18*(4), 1087, doi:10.1029/2003PA000920.

Stott, L., and A. Timmermann (2011), Hypothesized link between glacial/interglacial atmospheric CO_2 cycles and storage/release of CO_2-rich fluids from deep-sea sediments, in *Understanding the Causes, Mechanisms and Extent of Abrupt Climate Change*, *Geophys. Monogr. Ser.*, vol. 193, edited by H. Rashid, L. Polyak, and E. Mosley-Thompson, pp. 123–138, AGU, Washington, D. C.

Stott, L., J. Southon, A. Timmermann, and A. Koutavas (2009), Radiocarbon age anomaly at intermediate water depth in the Pacific Ocean during the last deglaciation, *Paleoceanography*, *24*, PA2223, doi:10.1029/2008PA001690.

Stuiver, M., and P. M. Grootes (2000), GISP2 oxygen isotope ratios, *Quat. Res.*, *53*, 277–284.

Stuut, J.-B. W., and F. Lamy (2004), Climate variability at the southern boundaries of the Namib (southwestern Africa) and Atacama (northern Chile) coastal deserts during the last 120,000 yr, *Quat. Res.*, *62*(3), 301–309.

Thornalley, D. J. R., S. Barker, W. S. Broecker, H. Elderfield, and I. N. McCave (2011), The deglacial evolution of North Atlantic deep convection, *Science*, *331*, 202–205.

Toggweiler, J. R., J. L. Russell, and S. R. Carson (2006), Midlatitude westerlies, atmospheric CO_2, and climate change during the ice ages, *Paleoceanography*, *21*, PA2005, doi:10.1029/2005PA001154.

van Geen, A., R. G. Fairbanks, P. Dartnell, M. McGann, J. V. Gardner, and M. Kashgarian (1996), Ventilation changes in the northeast Pacific during the last deglaciation, *Paleoceanography*, *11*, 519–528.

Weaver, A. J., et al. (2001), The UVic Earth System Climate Model: Model description, climatology, and applications to past, present and future climates, *Atmos. Ocean*, *4*, 361–428.

Wyrwoll, K.-H., B. Dong, and P. Valdes (2000), On the position of Southern Hemisphere westerlies at the Last Glacial Maximum: An outline of AGCM simulation results and evaluation of their implications, *Quat. Sci. Rev.*, *19*(9), 881–898.

Zahn, R., and A. C. Mix (1991), Benthic foraminiferal $\delta^{18}O$ in the oceans temperature-salinity-density field: Constraints on Ice Age thermohaline circulation, *Paleoceanography*, *6*(1), 1–20, doi:10.1029/90PA01882.